COAMPS wind validation in the NCOM Intra-American Seas (AMSEAS) domain in the Gulf of Mexico during 20 June to 10 July 2010, and the use of NCOM and COAMPS data to examine the impact of cyclones on the Deepwater Horizon oil spill

by

Pat Fitzpatrick, Yee Lau, Chris Hill, and Haldun Karan

Geosystems Research Institute

Mississippi State University

Overview

The Deepwater Horizon explosion reopened debate on the role of synoptic weather features versus ocean currents in transporting oil spills. Lagrangian models generally assume oil concentrations travel largely proportional (80-100%) to ocean currents' speed and direction, plus an additional 3% contribution from surface winds, diffused with each time step. However, cyclones are known to highly perturb water pollutants with positive and negative results. A mid-latitude cyclone expanded the Exxon Valdez oil spill over a large region, while in contrast Hurricane Henri (1979), in combination with a non-tropical low, cleansed the oil-polluted south Texas beaches (Gundlach et al. 1981).

We identified the late June to early July timeline as a period of interest since oil briefly impacted the Rigolets, Lake Borgne, and western Mississippi coast, and represented the innermost penetration of oil pollution east of the Mississippi River. An important component to understanding the oil transport is to distinguish the influences behind this apex moment. An oil spill simulation was conducted for the period 20 June to 10 July 2010 to understand this inland transport. Meteorology and ocean data, as well as synoptic maps also facilitated this analysis. The results of this analysis, as well as validation of numerical model wind analysis, are presented in this report. We also briefly discuss hydrology modeling software designed to predict the movement of oil pollution in the event of a hurricane landfall in the oil spill region at the end of this report.

Model overview

We developed a Lagrangian particle tracker with random walk diffusion to simulate the oil spill from 0000 UTC 20 June to 0000 UTC 11 July 2010 (Hunter et al. 1993; Dimou and Adams 1993). Input consisted of latitude and longitude parcel positions in the oil-contaminated area, wind, current, and an array of pseudo-random numbers. In addition, new parcels were released at the location of the damaged Macondo rig at each timestep. Twenty-five parcels were released at each position, and when combined with a 10 m^2s^{-1} diffusion coefficient, resulted in a natural trajectory spread with time. Initialization was based on NASA MODIS satellite imagery, SAR imagery from http://www.cstars.miami.edu, NOAA's Office of Response and Restoration oil trajectory maps at http://response.restoration.noaa.gov, and the NOAA/NESDIS Satellite Analysis Branch (SAB) experimental surface oil analysis products at http://www.ssd.noaa.gov/PS/MPS/deepwater.html. The parcels moved at 80% of the ocean current speed and at 3% of the wind speed[1]. Bilinear interpolation was applied at each timestep to determine the currents and winds at each parcel position.

---

[1] Sensitivity experiments were performed with the diffusion coefficient and current ratios. The chosen values reported herein provided the most accurate results. More work is underway using variational analysis to quantify the optimum weights for wind and ocean current influence on parcels movement.

The pseudo-random numbers were uniformly distributed between 0 and 1 and generated by the efficient Mersenne Twister algorithm (Matsumoto and Kurita 1998). This modern technique has passed stringent "diehard" and NIS tests for randomness, and will generate an incredibly long sequence of numbers ($2^{19937}-1$) before repeating. The initial seed was randomly obtained from machine noise (/dev/urandom on Linux machines).

The 10-m wind and near-surface currents were provided from an operational, data assimilating forecast system (Ko et al. 2003; 2008) run daily by the Naval Oceanographic Office called the Navy Coastal Ocean Model (NCOM). This version is simulated on the Intra-Americas Sea (AMSEAS) domain with a 3-km grid spacing, and covers the Gulf of Mexico, Caribbean, and western Atlantic. The AMSEAS data includes tidal components and a dynamic water surface which fluctuates from wind forcing even capable of capturing storm surge events (Korobkin et al. 2010). The Coupled Ocean-Atmosphere Prediction System (COAMPS) provided the atmospheric forcing (Hodur 1997; Chen et al. 2010). COAMPS grid spacing is 15 km and interpolated to NCOM's 3-km Cartesian grid. COAMPS wind stress was converted to wind speed by using a wind drag formula and assuming a drag coefficient of 0.001. The COAMPS winds and NCOM surface currents were used at initialization time up to 24-h forecasts, whereupon a new dataset was used from the next day.

COAMPS validation

COAMPS winds were validated against moored buoys and CMAN stations using standard error metrics and vector correlation[2]. Internal tests of three different vector correlation schemes (Hanson et al. 1992; Crosby et al. 1993 [also see Breaker et al. 1994]; Kundu 1976) showed the Hanson et al. algorithm possessed the best attributes: it provides parametric coefficients; it is invariant under rotation; it provides an angle of rotation as well as a scaling factor between two vector datasets; and is analogous to linear regression. With regard to the latter property, it provides a correlation coefficient between -1 and 1 as well as least square fit coefficients. The Hanson et al. scheme also quantifies vector reflection, although that property is irrelevant to meteorology validation.

An examination of bias and absolute errors during the summer study period show very small wind direction or speed bias, computed as buoys minus COAMPS (Table 1). However, COAMPS consistently underpredicted wind speed (to be discussed in a moment). The buoy/CMAN data were converted to 10-m height and 1-min averages for consistent comparisons[3]. The absolute errors for wind speed also are minimal, from 1.4 to 1.6 ms^{-1}. The wind direction absolute errors are small but not negligible from 31.0 to 37.9 deg; however, much

---

[2] It can be shown that vector correlation is a two-dimensional version of canonical correlation multivariate analysis.

[3] The 10-m adjustment was performed assuming a Charnock roughness length relationship and logarithmic wind profile. The 8-min average moored buoy winds were converted to 1-min average winds assuming a 9% gust factor increase.

of this error is due to the weak pressure gradients that favor variable winds during this period. An examination of COAMPS during a windy winter period containing several frontal passages (0000 UTC 1 December 2010 to 0000 UTC 15 January 2011) show similar error statistics except the wind direction absolute error is reduced by approximately 10 deg.

Other metrics and plot provide additional insight into the wind validation. Figure 1 shows the Hanson et al. methodologies and absolute error for wind validation at four offshore moored buoys. The "variance explained" ranges from 50 to 75%; most of the lost correlation is due to wind direction variability and the small model negative bias. The scalar factors are slightly greater than one, another indirect measure of model wind speed underforecasts. The rotation angles show equally small positive and negative values, another indication of no model wind direction bias. However, the wind direction absolute errors are less than the 37-buoy averages shown in Table 1. As will be shown, the larger wind direction errors are associated with coastal platforms.

Figure 2 depicts scatterplots of COAMPS data versus two offshore buoys. In general, the wind direction show a good positive linear correlation. However, while the wind speed scatterplots show a positive linear trend, a negative speed bias is evident. Furthermore, this bias increases with wind speed. Ovals representing one standard deviation of COAMPS and each buoy is shown in Fig. 2 for wind speed. Circular plots indicate both the model and buoys have the same data ranges, and elliptic plots indicate one dataset has less range than the other. Figure 2 shows generally elliptical patterns centered to the right, showing the NCOM negative speed bias.

Case studies were also performed to assess COAMPS initialization fields. A typical summertime example for wind direction and wind speed is shown in Figs. 3 and 4, respectively, for 0000 UTC 22 June 2010. They show generally small errors offshore with larger errors on the coast. Since the wind forcing of the oil spill is mostly dictated offshore, the mid-summertime COAMPS winds are deemed sufficiently accurate for utilization in the Lagrangian particle tracker model. Validation of the Gulf of Mexico flow features are underway by other scientists, but as will be shown, our examination of NCOM surface elevation data suggests the ocean model produces relatively accurate currents.

An appendix at the end of this report provides all the validation graphics for both the summer and winter COAMPS analyses.

Oil spill simulation analysis

Figure 5 shows four snapshots of the oil spill evolution simulated by the Lagrangian model for 20 June, 25 June, 30 June, and 5 July 2010, all at 0000 UTC. The first 8 days show two flow regimes: 1) east of the Mississippi River, oil moves northeast from the Macombo rig towards the Breton Sound islands, and the Alabama and west Florida coasts; and 2) west of the Mississippi River, a northwest current impacting the west Delta Region, Sandy Point Beach, Barataria Bay, Terrebonne Bay, and the shorelines/estuaries further west ending in the vicinity of Atchafalaya

Bay. Animations (not shown) include a pulsing action due to the diurnal tides common in this region. By the end of June, the simulation shows a sudden inward shift of the oil concentrations in western Mississippi Sound and Lake Borgne. A brief retreat occurs afterwards followed by a more prolonged inward penetration to these same regions.

Synoptic data analysis followed to clarify the cause of these two events. We examined scatterometer data, satellite/radar imagery, high-frequency radar (HFR) currents, COAMPS wind fields, buoy data, and North American surface map analyses. The HFR data (not shown) indicated a switch of eastward to westward currents off of Mississippi in late June, providing support that the NCOM ocean current changes were valid. An inspection of the weather maps shows a sequence of four distinct weather regimes that contributed to the two influxes of oil. A typical summertime pattern existed on 20 June, dominated by light winds and high pressure (Fig. 6; also see Figs. 3 and 4 for 22 June). Starting 25 June (Fig. 7) through 30 June (Fig. 8), a tropical system affected the Gulf as a tropical wave entered the region and eventually became Hurricane Alex. The tropical wave became a depression by 1800 UTC 25 June about 80 n mi north-northeast of Puerto Lempira, Honduras, moved west-northwestward, became a tropical storm on 0600 UTC 26 June, and made its first landfall in the Yucatan Peninsula near Belize City around 0000 UTC 27 June. The weakened tropical storm then re-entered the southwest Gulf, strengthened to a category 2 hurricane, and made its final landfall near Soto la Marina, in northeastern Mexico around 0200 UTC 1 July. It is during the period the first inward oil incursion happened into the Lake Borgne region.

Afterwards, a cold front moved offshore into the eastern Gulf of Mexico (Fig. 9), creating a northerly wind flow off in the northern Gulf Coast region. During this period, the oil retreated slightly. However, a non-tropical low pressure system formed on the western edge of this front (Fig. 10), and slowly moved westward then stalling south of eastern Louisiana (Fig. 11). This period is accompanied by a second oil incursion into the Mississippi Sound and Lake Borgne area. COAMPS analyses (Fig. 12) summarizes the wind patterns associated with these found weather regimes.

The fringe effect of Alex, as well as the close proximity of the non-tropical low, not only switched alongshore westerly coastal currents (not shown) to an easterly direction, but also increased inland water levels by 0.6 m to 0.8 m above normal as mini-surge events. The Shell Beach CMAN (Fig. 13, top) located in Lake Borgne, LA, shows peak water levels of 0.5 and 0.6 m above normal on 29 and 30 June, followed by slightly above normal conditions as the front pushed through, then a more prolonged elevated water period of 0.6-0.8 m above normal for 4-7 July. CMAN stations in Waveland, MS, and East Pascagoula, MS display similar patterns (not shown). NCOM captured these two elevated water periods in Lake Borgne (Fig. 13, bottom), but the magnitudes are too low. This is probably because the resolution cannot adequately capture the surge magnitudes this far inwards into the estuaries.

Development of operational storm surge modules for oil pollutant transport

These results thus far show that cyclones can dramatically alter oil transport, even by fringe effects. Indeed, the Northern Gulf Coast – especially the wetlands – may have escaped even worse oil pollution due to the lack of landfalling tropical cyclones in the Gulf of Mexico in 2010. Part of the deliverables involved developing a storm surge module for transporting oil pollutants in the event of tropical cyclone impact. This forecast system involved the Advanced CIRCulation (ADCIRC) hydrodynamic model to provide water currents and surge elevations, and the Lagrangian particle model discussed earlier for predicting oil transport.

An example of this system is shown in Figs. 14 and 15, which simulated the hypothetical scenario of a category 2 hurricane making a September landfall in Fourchon, LA. In September 2010, the beaches from Sandy Point to Chalon Pass, as well as northeast Barataria Bay (near Bay Jimmy), contained oiled shorelines as well imbedded oil on the sea bottom. It is assumed the oil remains on the bottom until a minimum velocity of 0.4 ms^{-1} is reached. In this scenario, oil would have been displaced westward, covering parts of Grant Isle, then moving northwards deep into the marsh north of Barataria Bay. The oil residual would have remained in the marsh as the surge retreated. Fortunately, this forecast system was never tested. It was also noted the results were sensitive to the initial displacement velocity. However, experiments with different diffusion coefficients yielded similar oil movement, just different dispersion spread widths.

Acknowledgments

References

Breaker, L. C., and W. H. Gemmill, 1994: The application of a technique for vector correlation to problems in meteorology and oceanography. *J. Appl. Meteor.*, **33**, 1354-1365.

Chen, S., T. J. Campbell, H. Jin, S. Gaberšek, R. M. Hodur, and P. Martin, 2010: Effect of two-way air–sea coupling in high and low wind speed regimes. *Mon. Wea. Rev.*, **138**, 3579–3602.

Crosby, D. S., L. C. Breaker, and W. H. Gemmill, 1993: A proposed definition for vector correlation in geophysics: theory and application. *J. Atmos. Oceanic Technol.*, **10**, 355-367.

Dimou, N. K., and E. E. Adams, 1993: A random-walk, particle tracking model for well-mixed estuaries and coastal waters. *Estuarine, Coastal, and Shelf Science*, **37**, 99-110.

Gundlach, E.R., K. J. Finkelstein, and J. L. Sadd, 1981: Impact and persistence of Ixtoc I oil on the South Texas Coast. *Proceedings: 1981 Oil Spill Conference (Prevention, Behavior, Control, Cleanup)*, March 2-5, 1981, Atlanta, GA. 477-485.

Hanson, B., K. Klink, K. Matsuura, S. M. Robeson, and C. J. Willmott, 1992: Vector correlation: Review, exposition, and geographic application. *Annals of the Association of American Geographers*, **82**, 103-116.

Hodur, R.M., 1997: The Naval Research Laboratory's Coupled Ocean/Atmosphere Mesoscale Prediction System (COAMPS). *Mon. Wea. Rev.*, **125**, 1414-1430.

Hunter, J. R., P. D. Craig, and H. E. Phillips, 1993: On the use of random walk models with spatially variable diffusivity. *J. Computational Physics*, **106**, 366-376.

Ko, D. S., R. Preller, and P. Martin, 2003: An experimental real-time Intra-Americas Sea Ocean Nowcast/Forecast System for coastal ocean prediction. *Proceedings of the 5th AMS Conference*

on Coastal Atmospheric and Oceanic Prediction and Processes, August 6-8, Seattle, WA, 97-100.

Ko, D.S., P. J. Martin, C.D. Rowley, and R. H. Preller, 2008: A real-time coastal ocean prediction experiment for MREA04, *J. Marine Systems*, **69**, 1728.

Korobkin, M., E. D'Sa, and D. S. Ko, 2011: Effects of Hurricane Ike on the Louisiana-Texas coast from satellite and model data. *Remote Sensing Lett*. **2**, 11-19.

Kundu, P. K., 1976: Ekman veering observed near the ocean bottom. *J. Physical Ocean.*, **6**, 238-242.

Matsumoto, M, and M. Saito, 2008: Mersenne twister: A 623-dimensionnally equidistributed uniform pseudorandom number generator. *ACM. Trans. On Modelling and Computer Simulation*, **8**, 3-30.

Table 1. Wind validation of COAMPS initialization and 6-, 12-, 18-h, and 24-h forecasts for 21 NCOM forecasts during 0000 UTC 20 June 2010 to 0000 UTC 10 July 2010. The average errors of bias and absolute error are based on 37 buoys and CMAN stations. The observations are adjusted to 1-min averages and 10-m height elevation. COAMPS' wind vector stresses are converted to wind speed u and v components assuming a drag coefficient of 0.001.

	Analysis	6-h	12-h	18-h	24-h
Wind direction bias (ms^{-1})	-2.6	-5.7	3.8	13.3	-4.8
Wind direction absolute error (deg)	33.6	31.0	37.9	35.7	33.6
Wind speed bias (ms^{-1})	-0.1	0.4	0.5	0.8	0.1
Wind direction absolute error (deg)	1.4	1.4	1.6	1.6	1.4

Table 2. As in Table 1, but for 46 NCOM forecasts during 0000 UTC 1 December 2010 to 0000 UTC 15 January 2011. The average errors of bias and absolute error are based on 23 buoys and CMAN stations.

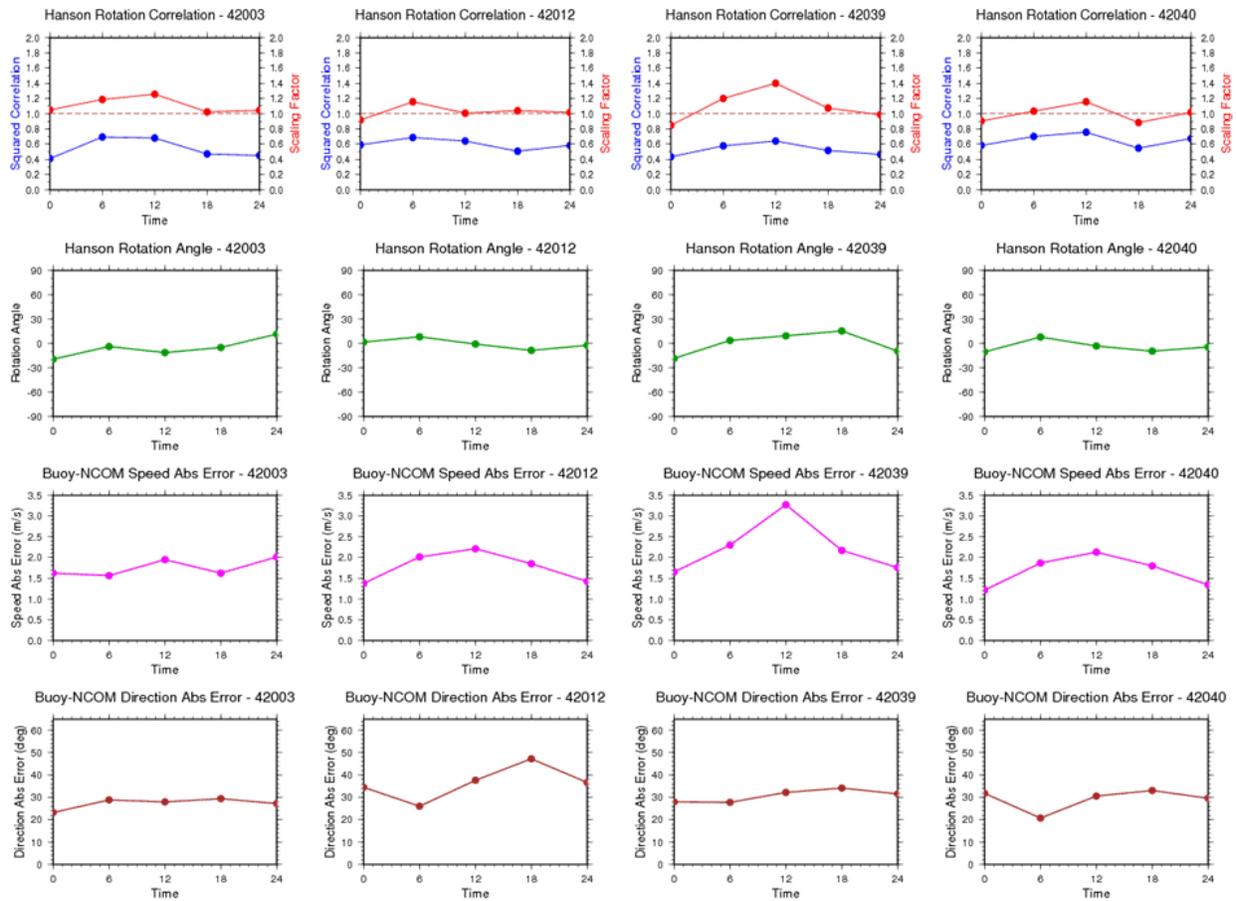|	Analysis	6-h	12-h	18-h	24-h
Wind direction bias (ms^{-1})	2.6	4.9	-2.6	1.7	1.8
Wind direction absolute error (deg)	26.0	22.1	21.8	28.1	26.2
Wind speed bias (ms^{-1})	0.7	0.4	0.4	0.9	0.8
Wind direction absolute error (deg)	1.8	1.7	1.7	1.6	1.8

Figure 1. Top two rows - Example of vector correlation squared, scaling factor, and rotation angle based on methodology of Hanson et al. (1992) for COAMPS winds initialization and forecast interpolated to 4 buoys (42003, 42012, 42039, and 42040), during the period 0000 UTC 20 June 2010 to 0000 UTC 10 July 2010. The dashed line corresponds to a squared correlation of 1. Bottom rows – absolute errors for wind direction and speed at the 4 buoys.
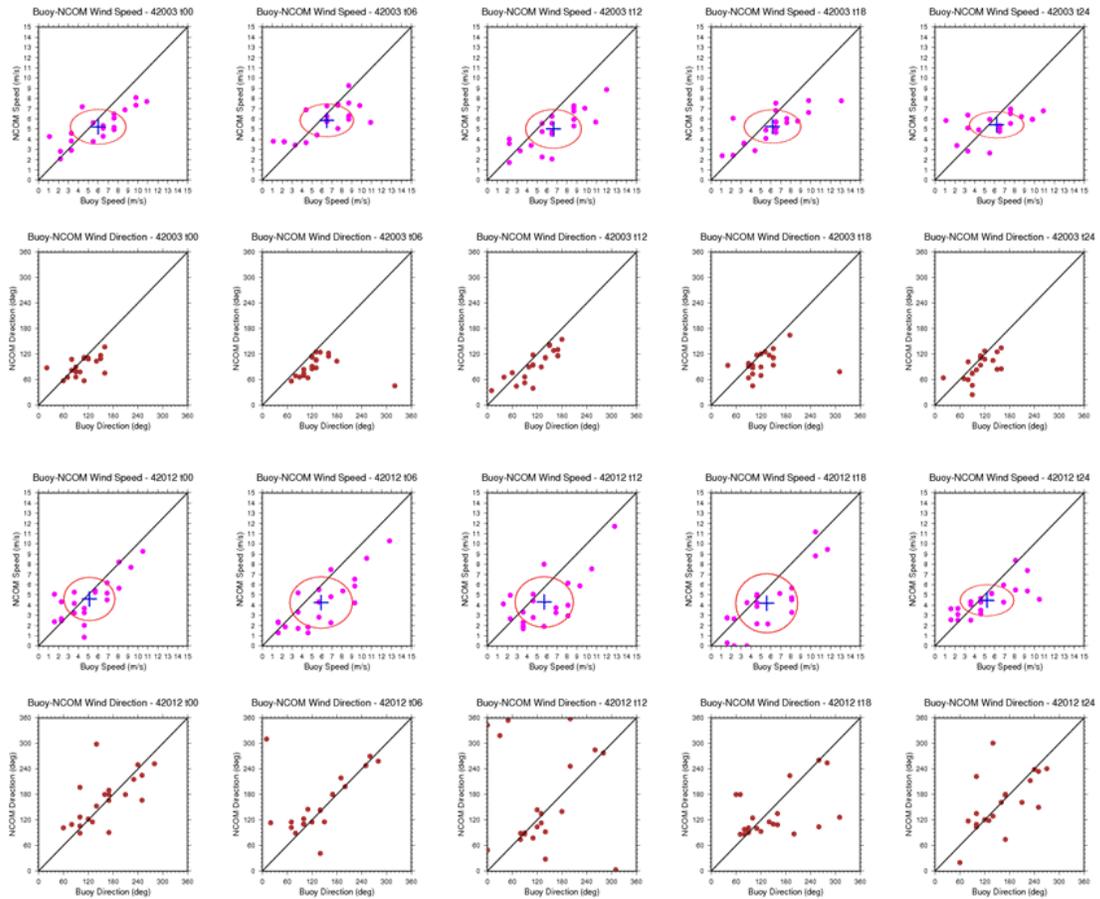
Figure 2. Example of scatterplots for COAMPS winds initialization and forecast interpolated to 2 buoys (42003 and 42012) during the period 0000 UTC 20 June 2010 to 0000 UTC 10 July 2010. Wind speed plots also include ovals representing one standard deviation of each dataset; circular plots indicate both the model and buoys have the same data ranges, and elliptic plots indicate one dataset has less range than the other.
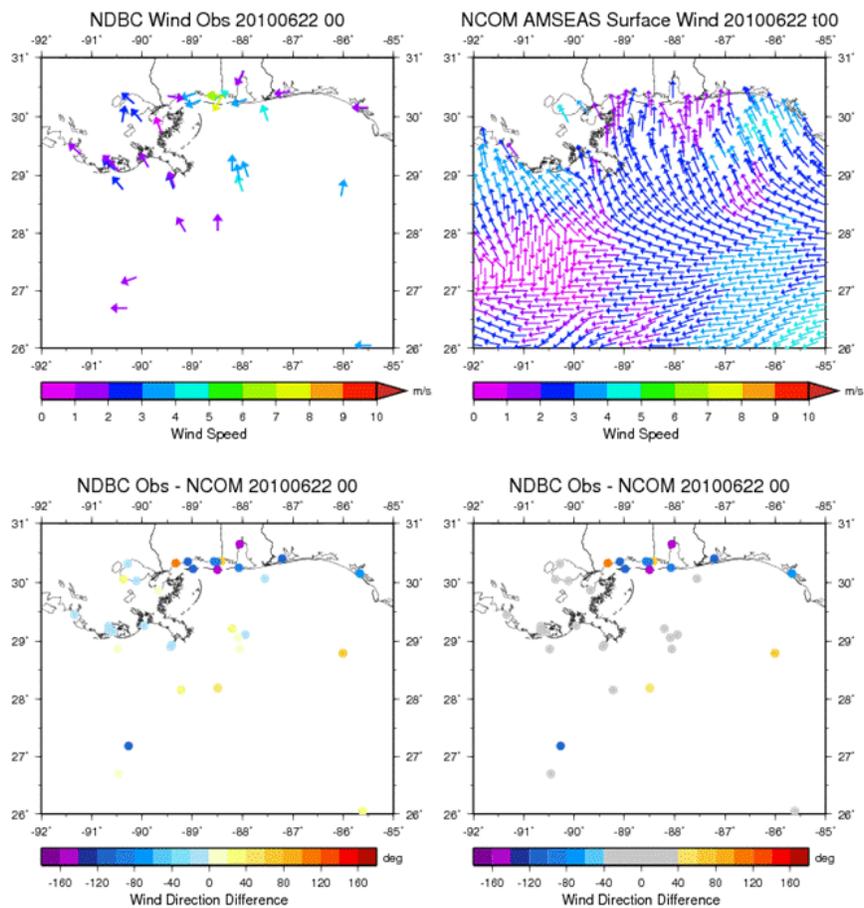
Figure 3. Example of a plot for daily analyses for COAMPS initialization for 0000 UTC 22 June 2010. Top left: Observed buoy vectors, shaded by wind speed. Top right: COAMPS wind vectors. Bottom left: Wind direction difference. Bottom right: same as bottom left, but "small" wind direction errors shaded grey.
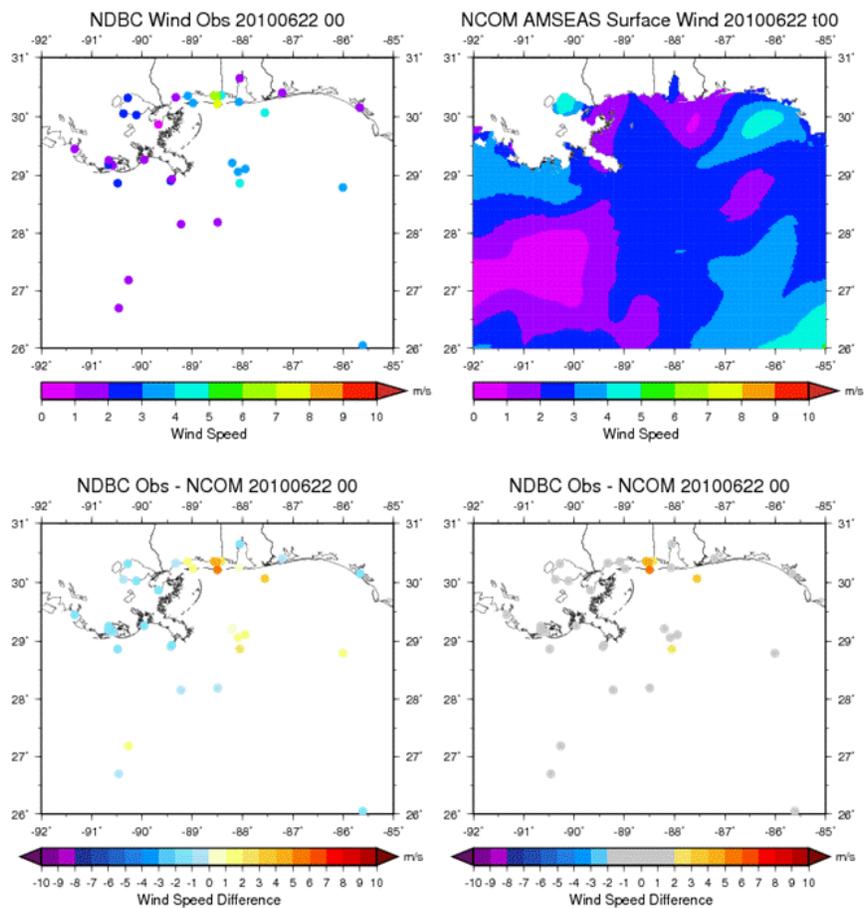
Figure 4. Example of a plot for daily analyses for COAMPS initialization for 0000 UTC 22 June 2010. Top left: Observed buoy wind speeds, shaded by wind speed. Top right: contours of COAMPS wind speed. Bottom left: Wind speed difference. Bottom right: same as bottom left, but "small" wind speed errors shaded grey.
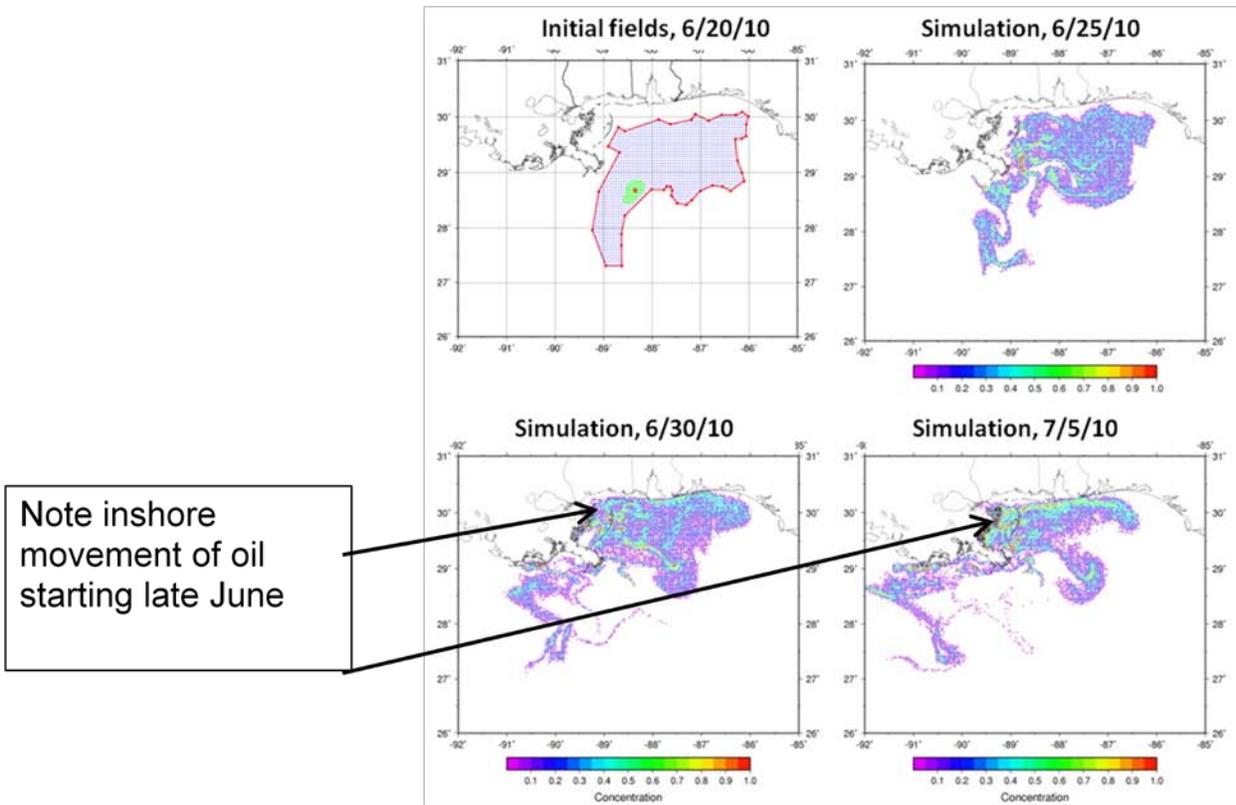
Figure 5. Snapshot images of the Deepwater Horizon oil spill simulation from 0000 UTC 20 June 2010 to 0000 UTC 10 July 2010. Note the inshore incursion into the Mississippi Sound and Lake Borgne regions starting in late June. Concentrations are computed as the ratio of parcels near a gridded point divided by the number of parcels originally released at each point. In these simulation, each point has 25 releases at initialization, then each trajectory is modified by a random number to mimic dispersion. Hence, concentrations in these runs are a fraction of 25.
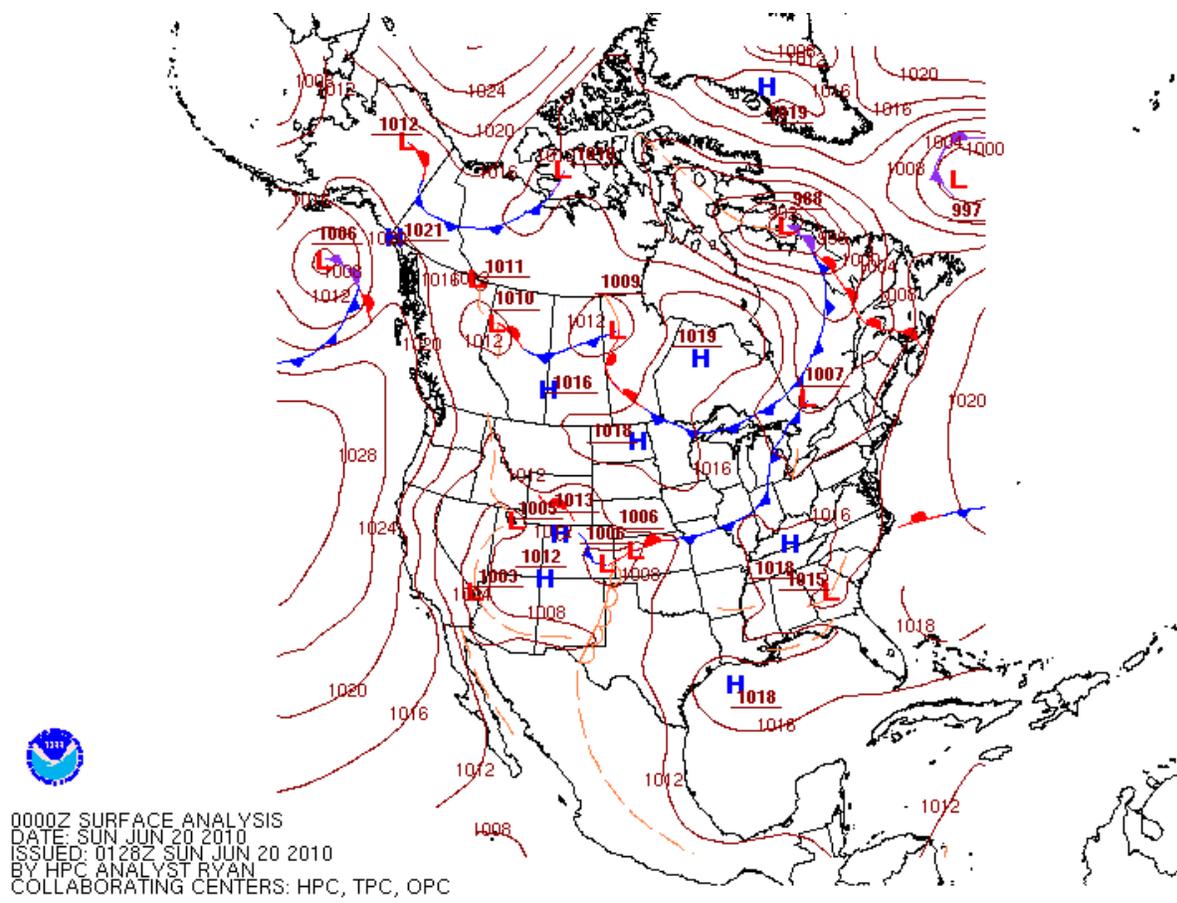
Figure 6. Hydrometeorological Prediction Center (HPC) North American surface analysis for 0000 UTC 20 June 2010 (available at http://www.hpc.ncep.noaa.gov/html/sfc_archive.shtml). HPC is part of the NOAA/National Weather Service National Centers for Environmental Prediction.
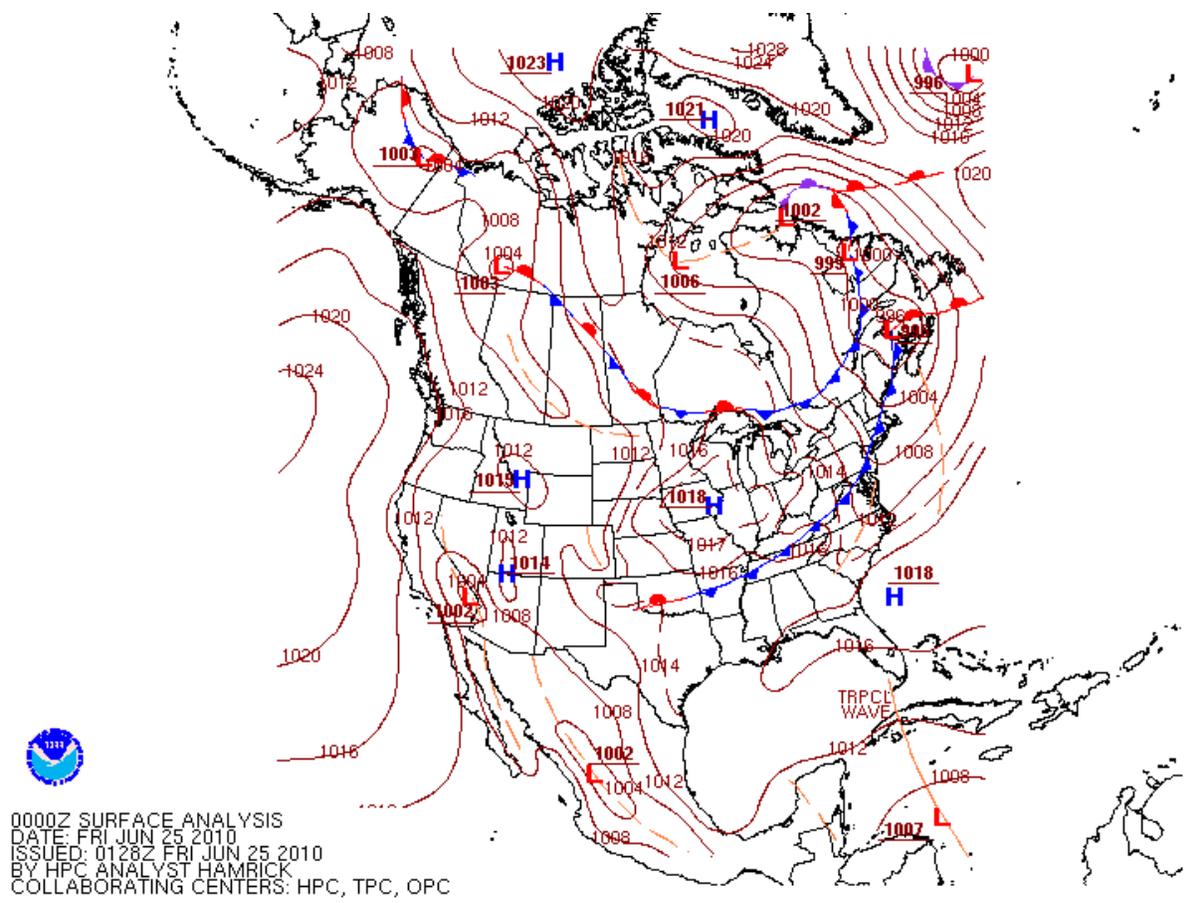
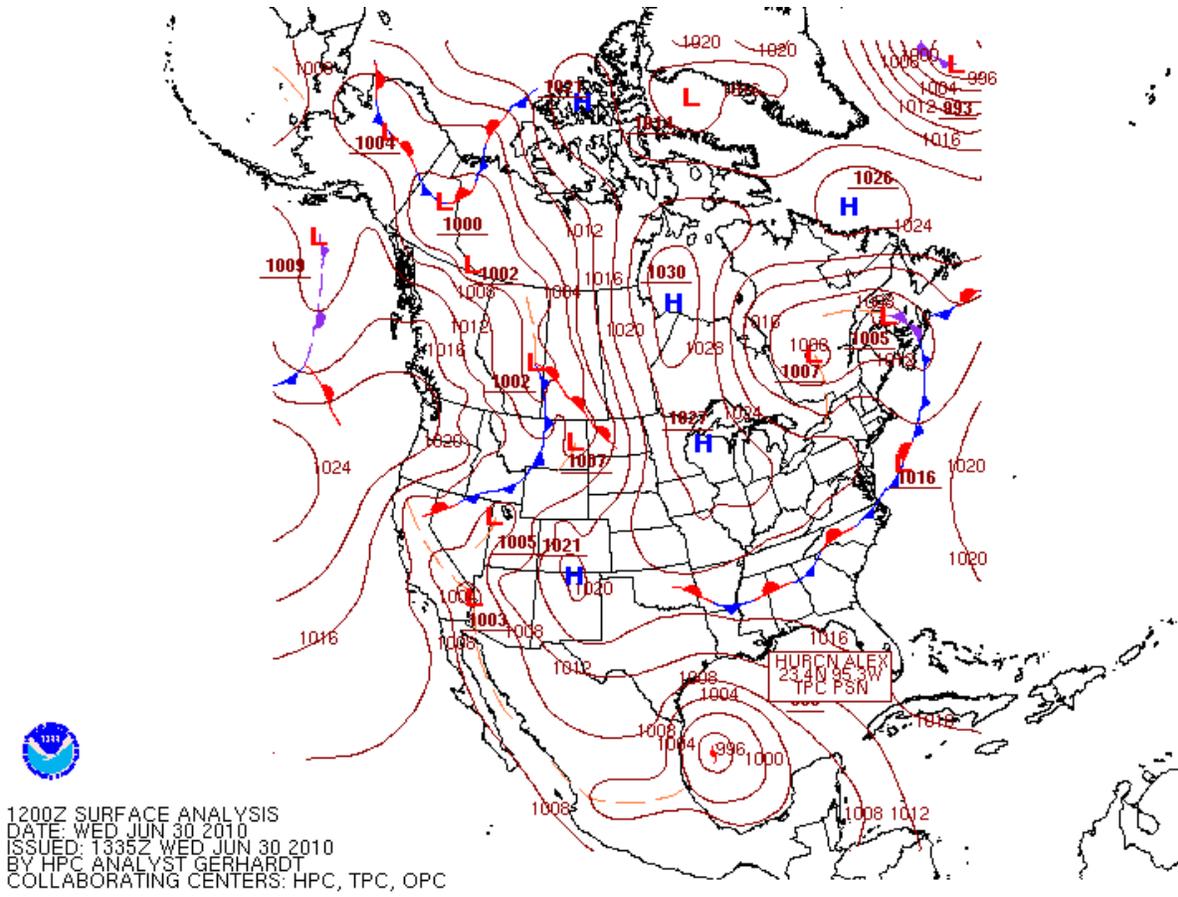**Figure 7. As in Fig. 6, but for 0000 UTC 25 June 2010.**

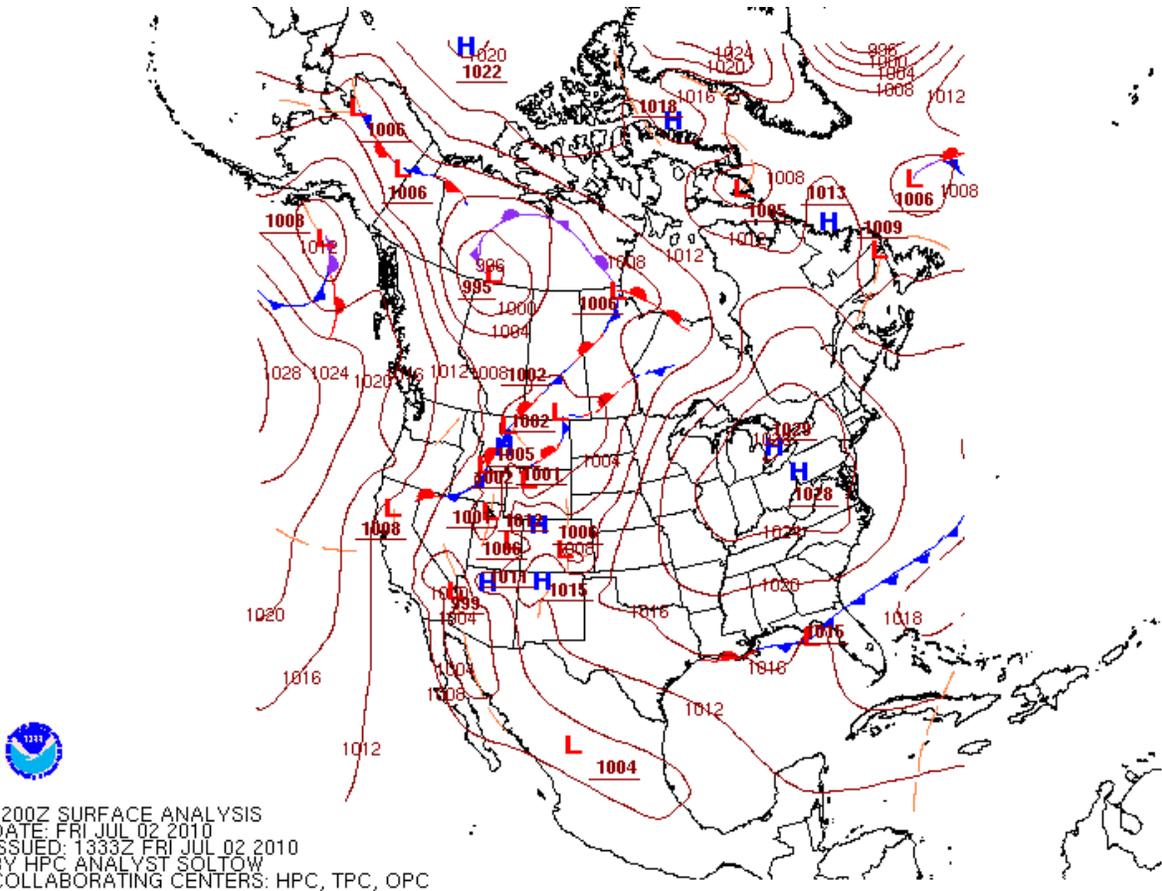Figure 8. As in Fig. 6, but for 1200 UTC 30 June 2010.

Figure 9. As in Fig. 6, but for 1200 UTC 2 July 2010.

0000Z SURFACE ANALYSIS
DATE: SUN JUL 04 2010
ISSUED: 0130Z SUN JUL 04 2010
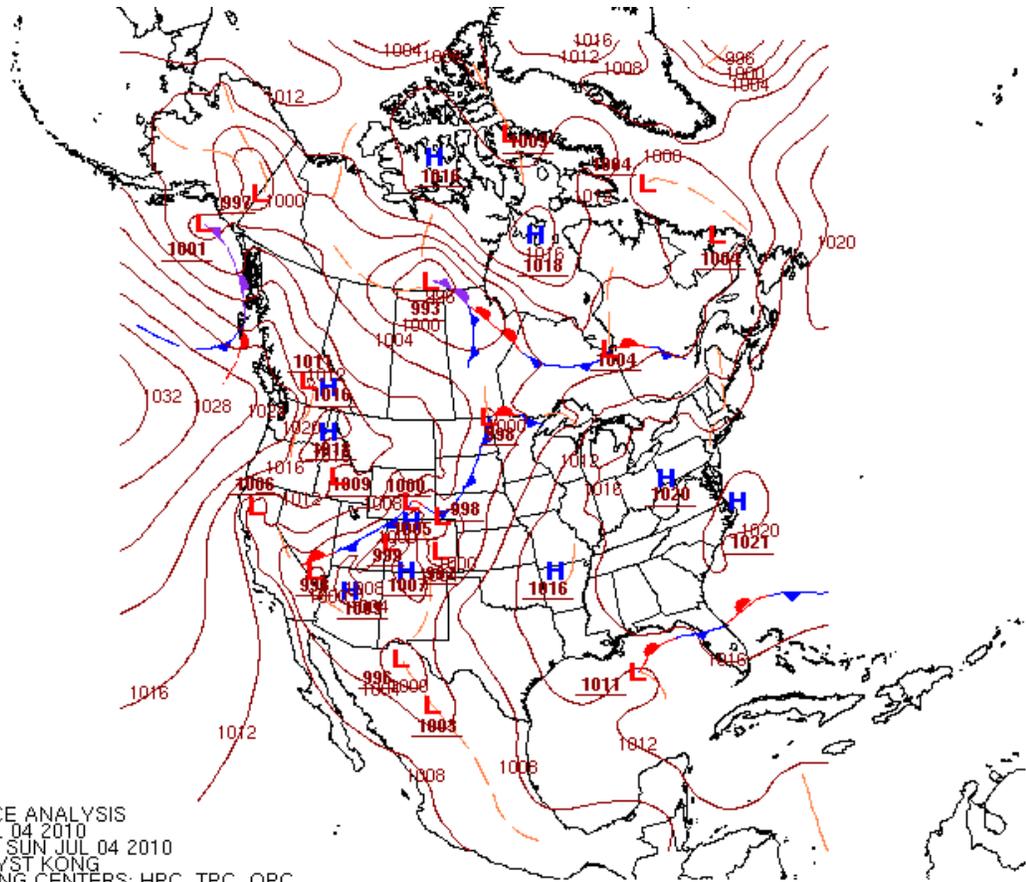BY HPC ANALYST KONG
COLLABORATING CENTERS: HPC, TPC, OPC

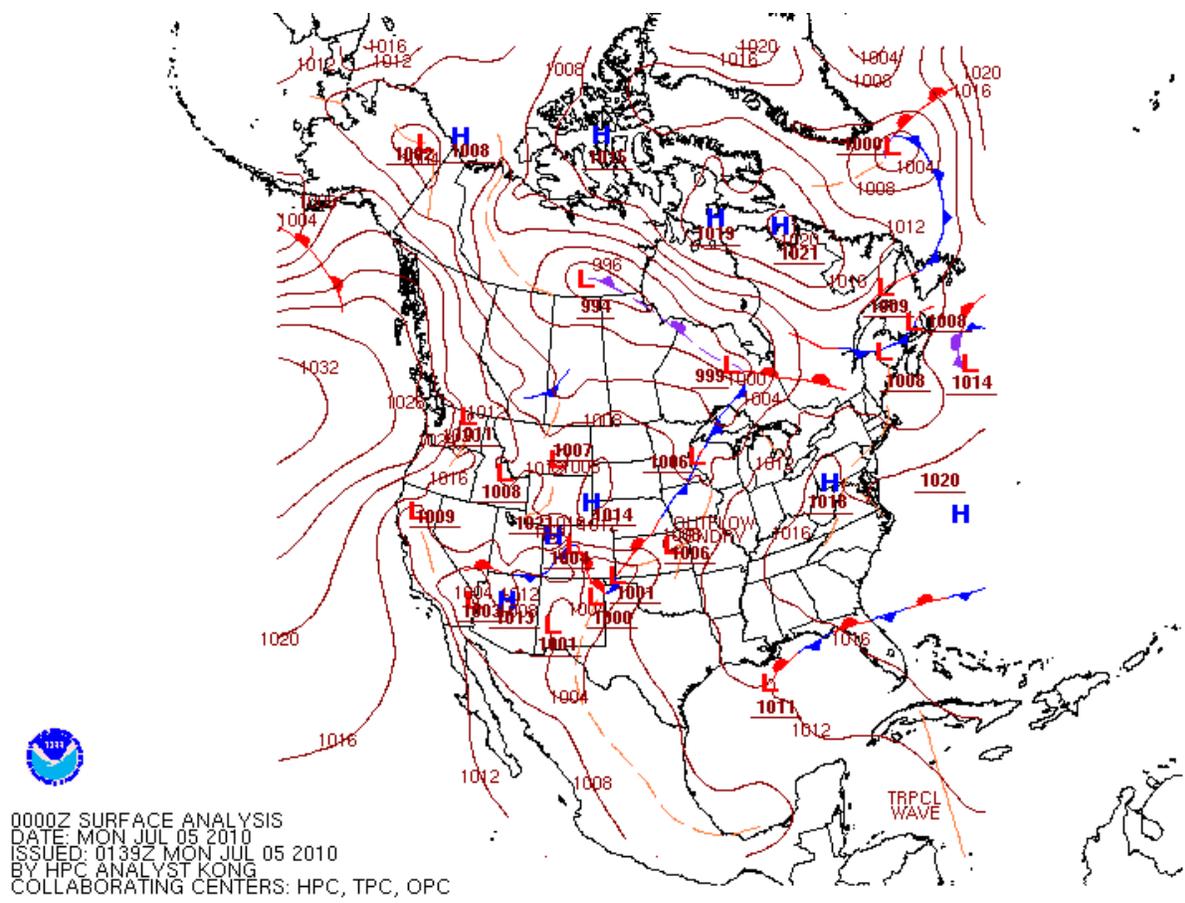**Figure 10. As in Fig. 6, but for 0000 UTC 4 July 2010.**

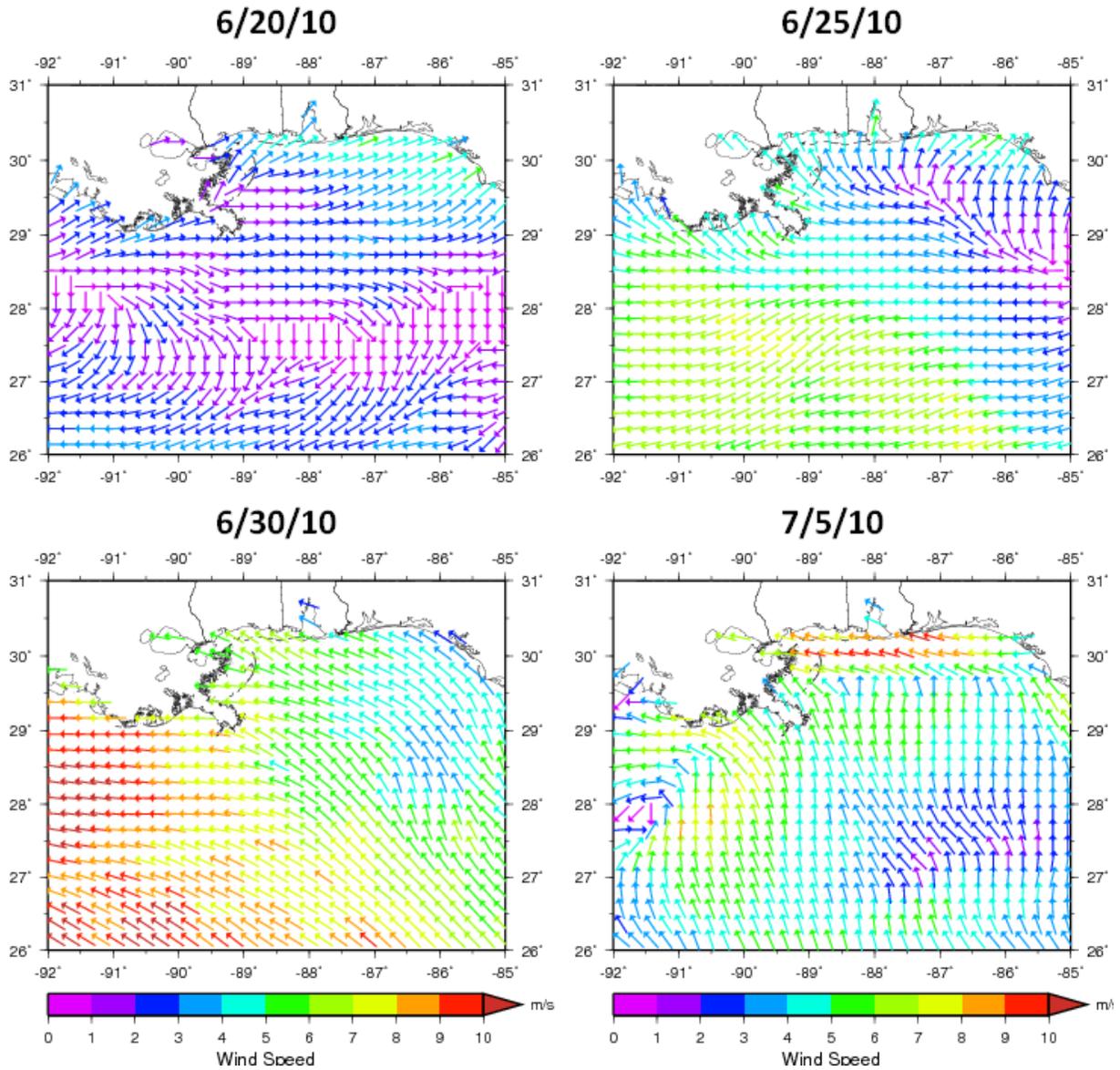**Figure 11. As in Fig. 6, but for 0000 UTC 2 July 5010.**

Figure 12. COAMPS winds for 0000 UTC 20 June, 25 June, 30 June, and 5 July 2010, depicting the weather regimes during this period. The period begins with typically weak summertime winds associated with a high pressure ridge (top left), then winds off of Mississippi becoming easterly associated first with a developing Tropical Storm Alex off of Yucatan, followed by fringe effects of category 2 Hurricane Alex as it approaches Mexico (lower left), concluding with an offshore cold front in the eastern Gulf (not shown) in which a non-tropical low forms on the front's western end and propagates south of Louisiana (lower right).
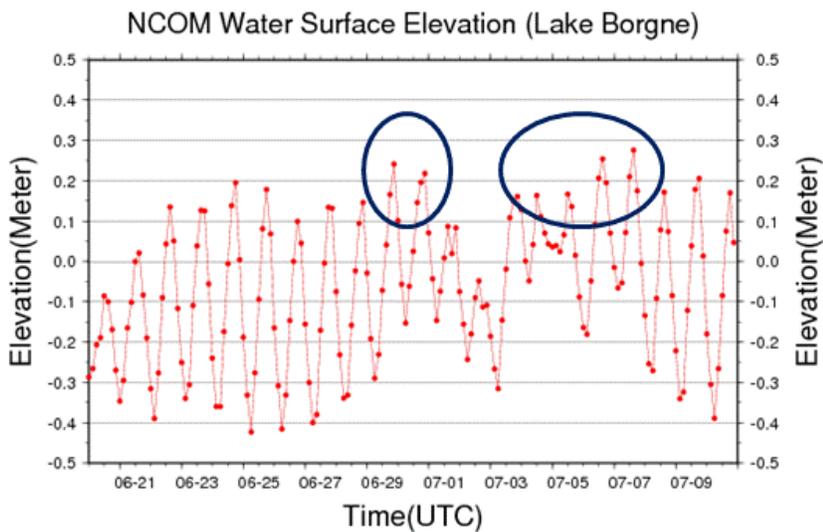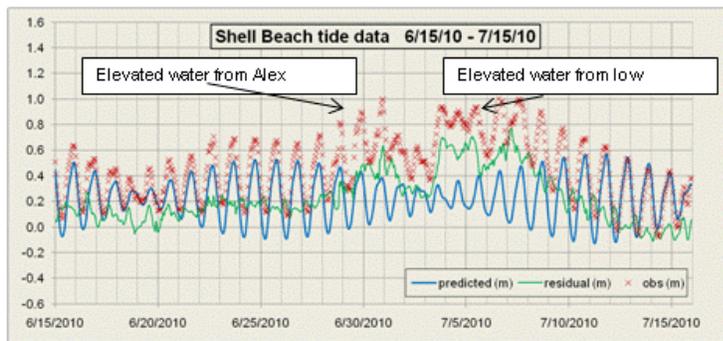
Figure 13. Top: Observed water level (red), tide prediction (blue), and residual (observed minus tide, in green) for Shell Beach CMAN station in Lake Borgne, LA, during 0000 UTC 15 June to 0000 UTC 15 July 2010. Bottom: NCOM surface elevation data for Lake Borgne from 0000 UTC 20 June to 0000 UTC 10 July 2010. Both plots indicate periods of above average water elevation   associated with Hurricane Alex and the non-tropical low pressure system. The observed water level data is archived at http://tidesandcurrents.noaa.gov/ (see links under "Verified Data" then "Coastal Stations").
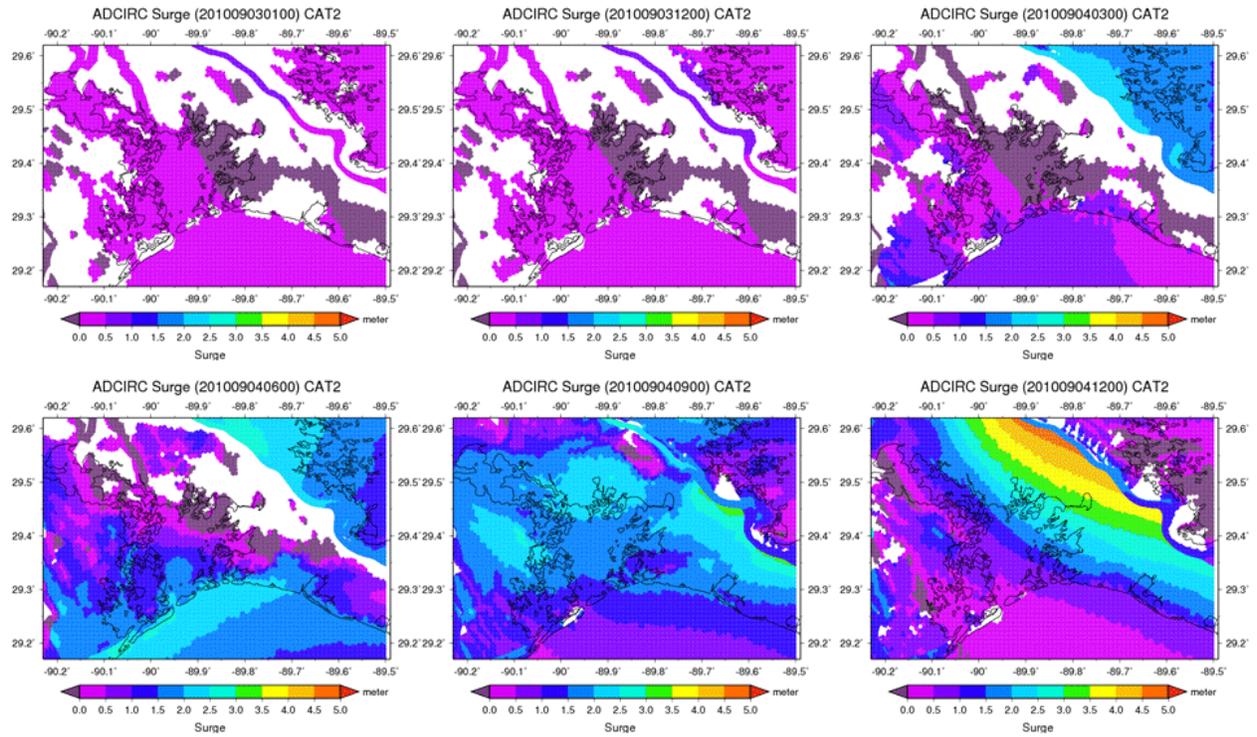
Figure 14. ADCIRC storm surge simulation of hypothetical category 2 hurricane making landfall in Fourchon, LA.
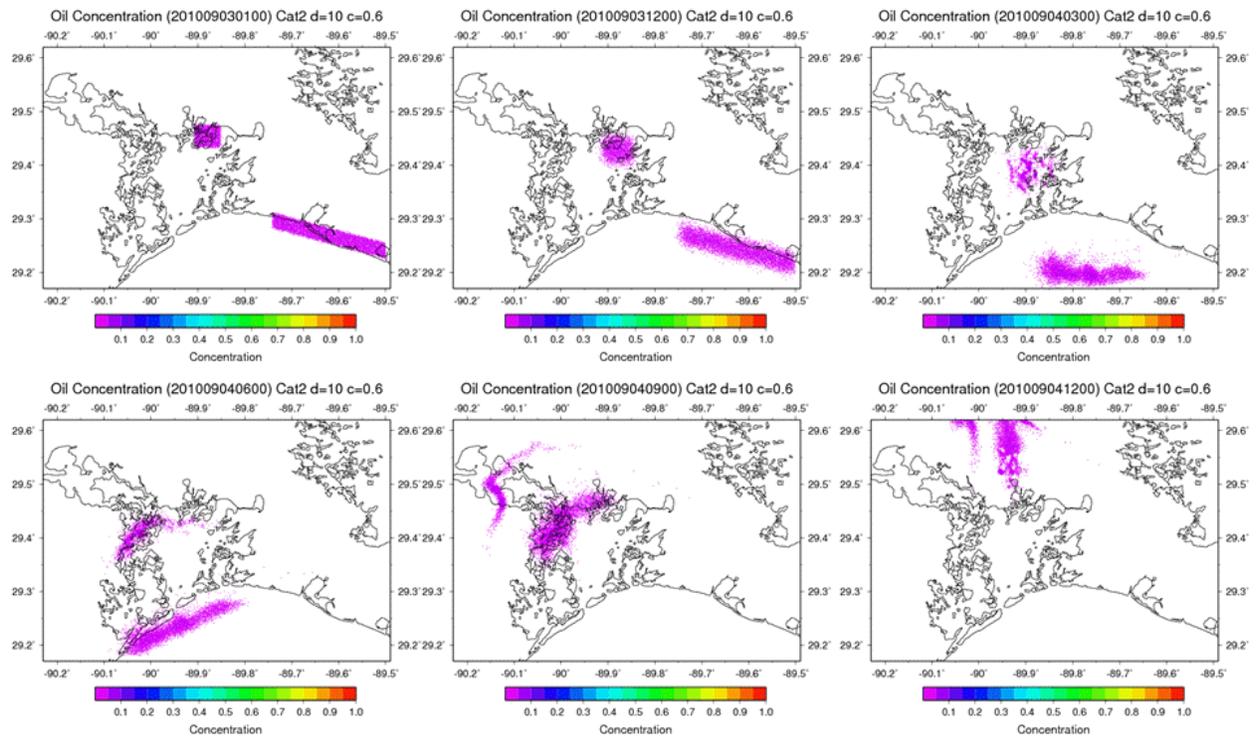
Figure 15. Displacement of oil from the beaches from Sandy Point to Chalon Pass and Bay Jimmy during storm surge depicted in Fig. 14.

Appendix: SURA Validation Plots,
Oil Spill Research Plots, Oil Spill Animation

The appendix files listed here are available in the accompanying supplemental materials archive.

Case study validations

Summer case study of COAMPS wind direction in northern Gulf of Mexico
Time frame: 0000 UTC 20 June 2010 to 0000 UTC 10 July 2010
Filename: BuoyNCOM_WindDirDiff_20100620-20100710.pdf

Summer case study of COAMPS wind speed in northern Gulf of Mexico
Time frame: 0000 UTC 20 June 2010 to 0000 UTC 10 July 2010
Filename: BuoyNCOM_WindSpdDiff_20100620-20100710.pdf

Winter case study of COAMPS wind direction in northern Gulf of Mexico
Time frame: 0000 UTC 1 December 2010 to 0000 UTC 15 January 2011
Filename: BuoyNCOM_WindDirDiff_20101201-20110115.pdf

Winter case study of COAMPS wind speed in northern Gulf of Mexico
Time frame: 0000 UTC 1 December 2010 to 0000 UTC 15 January 2011
Filename: BuoyNCOM_WindSpdDiff_20101201-20110115.pdf

Buoy/CMAN scatterplots

Scatterplots of COAMPS winds versus northern Gulf of Mexico buoys/CMANS
Time frame: 0000 UTC 20 June 2010 to 0000 UTC 10 July 2010
Filename: BuoyNCOM_SpdDir-PerStation-Scatter-MeanStdDev-20100620-20100710.pdf

Scatterplots of COAMPS winds versus northern Gulf of Mexico buoys/CMANS
Time frame: 0000 UTC 1 December 2010 to 0000 UTC 15 January 2011
Filename: BuoyNCOM_SpdDir-PerStation-Scatter-MeanStdDev-20101201-20110115.pdf

----

Validation metrics

Summer validation of COAMPS winds in northern Gulf of Mexico
Time frame: 0000 UTC 20 June 2010 to 0000 UTC 10 July 2010
Filename: RotCorrScalingFactor_RotAng_SpdDirAbsError_20100620-20100710_TimeSeries.pdf

Winter validation of COAMPS winds in northern Gulf of Mexico
Time frame: 0000 UTC 1 December 2010 to 0000 UTC 15 January 2011
Filename: RotCorrScalingFactor_RotAng_SpdDirAbsError_20101201-20110115_TimeSeries.pdf

----

Deepwater Horizon oil spill material

North American Synoptic Surface Map Analyses
Time frame: 000 UTC 20 June 2010 to 0000 UTC 10 July 2010
Filename: SFCANA_20100620-20100710.pdf

NCOM surface water elevations
Time frame: 000 UTC 20 June 2010 to 0000 UTC 10 July 2010
Filename: NCOMWaterSurfaceElevation-20100620-20100710.pdf

Satellite and radar imagery
Time frame: 000 UTC 20 June 2010 to 0000 UTC 10 July 2010
Filename: SFC-SAT_20100620-20100710.pdf

Example Category 2 surge and oil movement for landfall in Fourchon, LA
Filename: OilSpill-Current-Wind-Surge-Conc.pdf

Animation of Deepwater Horizon oil spill
Time frame: 000 UTC 20 June 2010 to 0000 UTC 10 July 2010
Filename: ncomOilConc_d10_c0.8_dense.wmv